# Nearest-neighbor distributions in $Ga_{1-x}In_xN_yAs_{1-y}$ and $Ga_{1-x}In_xN_yAs_{1-y-z}Sb_z$ thin films upon annealing

Vincenzo Lordi,* Homan B. Yuen, Seth R. Bank, Mark A. Wistey, and James S. Harris
*Solid State and Photonics Laboratory, Stanford University, Stanford, California 94305, USA*

Stephan Friedrich
*Advanced Detector Group, Lawrence Livermore National Laboratory, Livermore, California 94550, USA*
(Received 19 May 2004; revised manuscript received 6 December 2004; published 15 March 2005)

We examine the distribution of N-In nearest-neighbor bonds in GaInNAs(Sb) quantum wells (QWs) and observe quantitatively the evolution of the distribution during thermal annealing. We use near-edge x-ray absorption fine structure to compare the behavior of compressively strained quantum wells with relaxed thick-film samples, and find no significant effect of strain on the nearest-neighbor bonding. Photoluminescence (PL) and electroreflectance (ER) spectroscopies are used to quantitatively measure the distribution of N-In nearest-neighbor states for a series of variously annealed GaInNAsSb QW samples. We find that increased annealing temperature or time leads to a blueshift of the band gap that saturates after sufficient annealing. This saturation is related to a thermodynamic equilibration of the N-In nearest-neighbor bonding in the material toward highly In-coordinated states, from an as-grown material having a nearly random bonding arrangement dominated by N-Ga bonds. The different N-In nearest-neighbor states form a fine splitting of the band gap of the material. The average spacing between these levels is found to be considerably smaller for GaInNAsSb ($\sim$18 meV) than for GaInNAs ($\sim$35 meV). Furthermore, we present absorption measurements that reveal an increased optical efficiency of the higher In-coordinated N states that form upon annealing. Additionally, the line shape observed at room temperature in all of the spectroscopic measurements is Gaussian, indicating a strong exciton-phonon coupling in these alloys.

DOI: 10.1103/PhysRevB.71.125309 PACS number(s): 78.20.Ci, 61.10.Ht, 78.67.De, 81.40.Tv

## I. INTRODUCTION

The GaInNAs material system has received much attention over the past decade for its potential use in low-cost telecommunications optoelectronic devices operating in the 1.3–1.6 μm wavelength range.[1–3] The advantages of this material system stem from its ability to be grown on GaAs substrates and the possibility for monolithic integration of highly reflective distributed Bragg reflectors, which enable the fabrication of low-cost vertical cavity lasers as well as resonant cavity detectors and modulators. These devices can be applied in high volume to address the current bottlenecks in optical networks and also to enable low-voltage optical interconnects. Recent progress on the use of GaInNAs for these applications has succeeded in producing devices operating at up to 1.4 μm wavelength.[2,4] In the past few years, GaInNAsSb has been found to be a potentially superior material to GaInNAs for these applications, since higher quality material can be grown over the entire telecommunications wavelength range and particularly at the longest wavelengths that were previously unattainable. In addition, inherent advantages are expected for GaInNAsSb over the competing material grown on InP (InGaAsP), due to a heavier electron effective mass, better electron confinement in quantum wells, and higher differential gain. High-performance device characteristics have been demonstrated with GaInNAsSb for wavelengths spanning the 1.3–1.6 μm range.[5–8]

Understanding the intricacies of the atomic structure and bonding in these dilute nitride materials is important for both improving the material quality and understanding the unique properties they exhibit, such as the blueshift of the band gap upon thermal annealing and the giant reduction of the band gap upon addition of small amounts of N.[9–15] We have recently used x-ray absorption spectroscopy (XAS) to directly examine the N-In nearest-neighbor bonding in thick films of $Ga_{0.7}In_{0.3}N_{0.03}As_{0.97}$ and probe how it changes with annealing.[9] A shift in the nearest-neighbor distribution toward increased N-In bonding was found to occur and to correspond to a thermodynamic stabilization of the material as well as to the observed blueshift in the band gap.

In this paper, we examine first the effect of biaxial compressive strain, which is present in the technologically relevant thin films used in optoelectronic devices, on the N-In nearest-neighbor bonding, using XAS. We find that strain does not alter the random nature of bonding in as-grown material nor does it change the atomic reconfiguration behavior upon annealing. We also observe the N-In nearest-neighbor states in thin-film GaInNAsSb material, using various spectroscopic techniques, including photoluminescence, electroreflectance, and optical absorption. The presence of Sb (a Group V element) is found not to affect the N-In bonding to first order. With electroreflectance we are able to distinguish each of the N-In nearest-neighbor states and extract bonding distributions in a series of partially annealed quantum well samples. Assignments of individual bonding states in the spectra are possible by using the results of the XAS experiments and *ab initio* band-structure calculations. We find that, like GaInNAs, as-grown GaInNAsSb material contains a nearly random distribution of N-In bonds, while annealing drives the material toward a state with increased N-In bonding and a larger band gap. The evolution of these states is monitored quantitatively during annealing.

 

Furthermore, we attribute an observed saturation of the band gap blueshift with increased anneal to the achievement of thermodynamic equilibrium of the nearest-neighbor distribution, consistent with our model of the mechanism for the blueshift. Finally, by the analysis of absorption spectra, we determine that the higher N-In bonded annealed material has increased optical efficiency (stronger matrix element) relative to the mostly N-Ga bonded as-grown material. While the large increase in photoluminescence intensity observed after annealing is mostly attributable to the removal of nonradiative recombination centers, the effect of increasing the matrix element for radiative recombination is also an important intrinsic property of the crystalline material.

## II. EXPERIMENTAL DETAILS

GaInNAs(Sb) samples were grown using solid-source molecular beam epitaxy (MBE) with nitrogen supplied by a radio frequency plasma cell. Arsenic and antimony were supplied by solid cracker cells (valved and unvalved, respectively). The active regions were grown with substrate temperatures of 420–455 °C, while GaAs regions were grown at ~600 °C. Details of the growth are described elsewhere.[6] GaInNAs samples were rapid thermal annealed in $N_2$ ambient at 760–800 °C for 1–2 min after growth, while GaInNAsSb samples were annealed at 760–800 °C for 1–3 min. GaAs proximity caps were used to prevent As desorption during annealing. Typical compositions of GaInNAs quantum wells (QWs) were 30% In and 1.6% N, with 2% N in the barriers; GaInNAsSb QWs were ≈40% In, 2.5% N, and 2.7% Sb, with 2.7% N in the barriers.

Nitrogen *K*-edge near-edge x-ray absorption fine-structure (NEXAFS) spectra were obtained at beam line 4.0.2 of the Advanced Light Source[16] using fluorescence detection with a high-resolution superconducting tunnel junction x-ray detector operated at ~0.1 K.[9,17] GaInNAs thin-film samples for NEXAFS consisted of uncapped 100 Å films grown on top of GaAs buffers on *n*+ GaAs substrates.

Diode samples consisted of a 1.38 μm thick $1\times10^{18}$ $cm^{-3}$ Si-doped GaAs *n*-type region followed by a 0.5 μm thick GaAs nominally intrinsic region ($\lesssim1\times10^{15}$ $cm^{-3}$ *n* type) and 1.0 μm of $5\times10^{17}$ $cm^{-3}$ Be-doped GaAs *p*-type region, all grown on a semi-insulating GaAs substrate. GaInNAs(Sb) quantum wells (8 nm thick) with GaNAs barriers (20 nm thick) were grown in the center of the *i* region, maintaining its total 0.5 μm thickness. Test devices were fabricated by depositing Ti/Pt/Au top ring contacts, etching circular mesas down to the middle of the *n* region, and depositing Au/Ge/Ni/Au bottom ring contacts. A well-defined optical aperture was left in the top contact. The *n*-type contact was alloyed at 400 °C for 45 s.

Photoluminescence (PL) was excited by the 488 nm line of an $Ar^+$ laser focused on the QWs through the *p*-doped layer, and PL spectra were collected with a Newport 818-IG InGaAs photodiode placed after an Acton SpectraPro 300i 0.3 m grating spectrometer. Absorption spectra were obtained using the photocurrent (PC) method, with electrical bias applied in series with the device and ammeter. The input illumination was chopped at 307 Hz and PC detected with a lock-in amplifier. Values for absorption coefficient were calculated from PC by assuming the maximum internal quantum efficiency (at high temperatures and biases) was 100%, and including both QWs and barriers in the interaction length. Interference effects of the multilayer structure on the illumination intensity were included in the calculation by using measured reflectivity spectra.[7] Electroreflectance (ER) spectroscopy was performed at near-normal incidence and detected with a calibrated InGaAs photodiode using phase-sensitive detection. A positive square wave ac modulation of 200 mV (307 Hz) was applied across the diode samples on top of the applied dc bias. The magnitude of the ac modulation was chosen to maximize the signal-to-noise ratio of the measured ER spectra, while verifying that the spectra were unchanged from those taken with smaller ac modulations. The spectra were also verified to be essentially independent of incident angle. Illumination for PC and ER was provided by a 250 W quartz-tungsten-halogen white light passed through a 950 nm long-pass filter and a 0.25 m grating monochromator, then coupled into a quartz fiber bundle before being focused onto the sample. The illumination for ER experiments was aligned onto the sample by maximizing the PC signal.

## III. RESULTS

### A. Near-edge x-ray absorption fine structure (NEXAFS)

We have previously shown, using x-ray absorption spectroscopy of both the N *K*-edge and In *K*-edge of bulk GaInNAs having similar composition as the material in this study, that thermal annealing causes an increase in the degree of N-In bonding.[9] Primarily from the magnitude of measured core-level shifts in the N-*K* NEXAFS spectra, compared with a GaNAs reference, it was determined that as-grown unstrained GaInNAs material contains a nearly random distribution of N-In bonds. This result indicated a kinetic product for the as-grown material, as expected from the low growth temperature. *Ex situ* thermal annealing resulted in a material with increased number of N-In bonds as it was driven toward thermal equilibrium. *Ab initio* total energy and band-structure calculations predicted an increased stability, as well as a blueshift in the band gap, as the degree of N-In bonding increased. The results agreed well with an observed blueshift of the peak emission wavelength in PL upon annealing. The reader is referred to Ref. 9, for details of the experiments and analysis.

In this current work, the experiments and analysis described above for unstrained thick-film samples were repeated on strained thin-film samples of GaInNAs having essentially the same composition. The experimental procedure for obtaining N-*K* NEXAFS was identical to that used in Ref. 9 except longer acquisition times were necessary to achieve comparable signal-to-noise ratios. The same basic conclusions were reached: despite strain in the film, the as-grown material contained a nearly random distribution of bonds, while the material annealed at 800 °C for 2 min showed an increase in the degree of N-In bonding toward a distribution peaked at two or three N-In bonds per N atom.

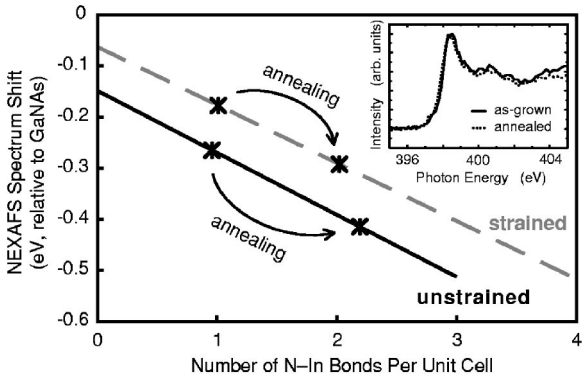


FIG. 1. Measured spectrum shifts (symbols) in N *K*-edge NEXAFS, relative to GaNAs, plotted on top of theoretical curves (lines) showing the predicted dependence on N nearest-neighbor environment, for both strained and unstrained GaInNAs. Arrows indicate transitions from as-grown to annealed material. Inset: representative NEXAFS spectra from the thin-film GaInNAs samples.

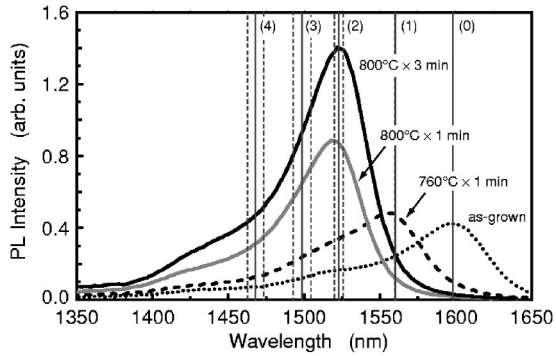


FIG. 2. Room-temperature photoluminescence spectra from GaInNAsSb QWs, both as-grown and annealed to various degrees. The solid vertical lines indicate the N-In nearest-neighbor peak fit positions, while the dashed vertical lines demarcate one standard deviation of error for the peak positions.

Proper analysis of the present data required repeating the supercell calculations to account for strain. Calculations were performed on 64-atom model supercell structures denoted by GaInNAs$^{(n)}$, where $n$ denotes the number of In atoms surrounding each N in the model. Details of the parameters used in the computations, which utilized ultrasoft pseudopotentials, are given in Ref. 9. To account for the biaxial compressive strain in the film resulting from growing pseudomorphically on a GaAs substrate, the lattice constant in the two in-plane directions were fixed to that of GaAs for each model. Relaxations were then performed to determine the out-of-plane lattice constant and equilibrium atom positions, before performing calculations of band structure, partial local density of states, and core-level shifts. The Poisson's ratio determined using this method ($\sim$0.34) agrees within 4% of that obtained using Vegard's law (linear combination of the elastic constants $C_{11}$ and $C_{12}$ of the endpoint binaries).

The main measurement result of the thin-film NEXAFS experiments is the magnitude of the N *K*-edge spectrum shift, relative to GaNAs, for as-grown and annealed material. However, further details of the measurements, calculations, and analysis will be presented elsewhere.[18] The measured values of spectrum shift are compared to theoretical predictions for N-In nearest-neighbor configurations, with the theory accounting for core-level shifts and differences in conduction band offsets.[9] The theory predicts smaller spectrum shifts for strained material than for unstrained material, for comparable arrangements of nearest neighbors. Figure 1 summarizes the results of these measurements and calculations. The straight lines indicate the predicted spectrum shifts, relative to GaNAs, for the different configurations of N-In nearest neighbors in GaInNAs with $\sim$30%In and $\sim$3%N, for both unstrained and strained material. The measured shifts for as-grown and annealed material are plotted as symbols on top of the theoretical curves to determine the dominant bonding configuration. The arrows in Fig. 1 indicate the transition from as-grown to annealed material. Some uncertainty in the calculations exists from the difficulty in accurately determining conduction band offsets, and a measurement error on the order of a couple of symbol widths also exists, but the general conclusions are clear. As-grown material is dominated by GaInNAs$^{(1)}$ bonds (a random distribution), while annealed material contains an increase in N-In bonding (toward thermodynamic equilibrium). Little difference is observed in the bonding distributions between strained and unstrained material. Furthermore, these samples show signs of "incomplete" annealing, with further shifts in the nearest-neighbor bonding possible. This fact is explained more clearly below.

### B. Photoluminescence (PL)

That thermal annealing causes a blueshift in the peak PL wavelength of these materials is a well-known phenomenon.[19–21] Our own calculations[9,22] and those of others[11] show that this band gap shift is related to N-In nearest-neighbor rearrangements in GaInNAs. We see a similar effect with GaInNAsSb.

At low temperatures, the PL spectra of GaInNAsSb samples show a symmetrical line shape, or a slight shoulder on the low-energy side arising from the $\exp(-\hbar\omega/kT)$ term in the van Roosbroek–Shockley relation for band-to-band recombination.[23] However, as the temperature is raised, carriers are thermally excited to higher energy levels in the material and at room-temperature high-energy ripples are present in the PL spectra. These high-energy features are more pronounced for as-grown material. Increasing the excitation density in the PL experiment is not effective in filling these states, since the density of states of a QW is very high at the band edge. This is evidence that the high lying states are not merely spatially localized inhomogeneities.

The PL experiments were performed on a series of GaInNAsSb QW samples: as-grown, annealed at 760 °C for 1 min, annealed at 800 °C for 1 min, and annealed at 800 °C for 3 min. Increasing the thermal dose results in increased PL intensity, but also more significantly a blueshift of the peak wavelength. However, after a certain dose, the wavelength

ceases to shift, as shown in Fig. 2. Similar behavior is observed for GaInNAs samples as well.

The peaks and shoulders in the PL spectra at room temperature can be fitted very well using Gaussian line shapes, which is somewhat unexpected; in fact, the signal from the GaAs substrate is well fit by a single Lorentzian line. However, a Gaussian line shape is observed for GaInNAs(Sb) at room temperature in all of the techniques described in this paper, as well as in electroluminescence (not presented). The Gaussian line shape indicates a strong exciton-phonon coupling in the material, arising from a large exciton effective mass, relatively large exciton radius, and inherent lattice defects in the alloy.[24]

A set of exactly five peaks common to all of the PL spectra is found by independently fitting each spectrum with the least number of Gaussian curves that result in a reasonable fit. These peak positions are indicated by the vertical lines in Fig. 2 (with $1\sigma$ deviations indicated by the dashed vertical lines) and will be shown more conclusively below to correspond to the five N-In nearest-neighbor configurations in the material. The peaks show a spacing of 17–20 meV and have full width at half maximum (FWHM) of 20–25 meV. The peak fitting described here was possible because the light hole transitions in this material are separated from the heavy hole transitions (appearing in PL) by a large energy ($>$120 meV), eliminating complications from overlap of the two sets of transitions. This will be a very important fact in the analysis of the ER spectra below.

### C. Electroreflectance (ER)

Electroreflectance is a sensitive modulation spectroscopy technique that probes critical points in the band structure with a scanned-energy probe beam, thus being equally sensitive to ground and excited states, unlike PL. The technique measures derivatives of the dielectric function via the expression

$$\Delta R/R = a\Re(\Delta\epsilon) + b\Im(\Delta\epsilon), \tag{1}$$

where $\Delta R/R$ is the measured modulated reflectivity, $a$ and $b$ are the Seraphin coefficients, and $\Delta\epsilon$ is the modulated dielectric function resulting from, in our case, modulation of the applied electric field (voltage) across the QWs.[25] For isolated QWs experiencing a change in electric field $\Delta\mathcal{E}$, $\Delta\epsilon$ can be written as[26]

$$\Delta\epsilon = \left(\frac{\partial\epsilon}{\partial E_0}\frac{\partial E_0}{\partial\mathcal{E}} + \frac{\partial\epsilon}{\partial\gamma}\frac{\partial\gamma}{\partial\mathcal{E}} + \frac{\partial\epsilon}{\partial I}\frac{\partial I}{\partial\mathcal{E}}\right)\Delta\mathcal{E}, \tag{2}$$

where $E_0$ is the transition energy, $\gamma$ is a broadening parameter, and $I$ is the integrated intensity of the transition. To proceed, a line shape needs to be assumed; from our PL, absorption, and electroluminescence measurements, we know that a Gaussian line shape is appropriate. Furthermore, in the vicinity of the fundamental energy gap of semiconductors, $b \ll a$, so for our analysis Eq. (1) reduces to[25]

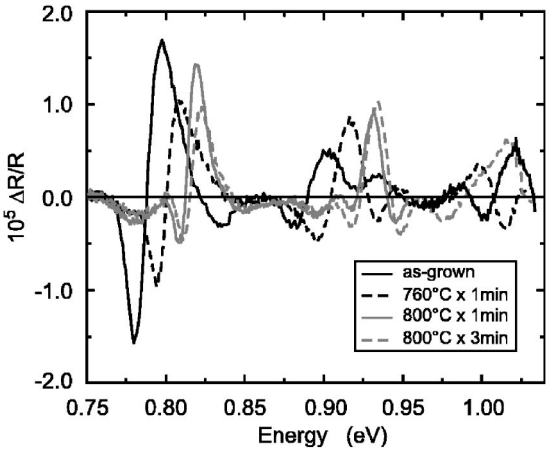


FIG. 3. Room temperature electroreflectance spectra taken from variously annealed GaInNAsSb QWs.

$$\Delta R/R \propto \Re(\Delta\epsilon). \tag{3}$$

The latter two terms in Eq. (2) can be lumped together, and following Shen *et al.*, assuming a normalized Gaussian line shape, the modulated reflectivity can be written as[27]

$$\Delta R/R = A(1/\gamma^2)\Phi(1, 0.5, -0.5x^2) + B(2x/\gamma^2) \times \Phi(2, 1.5, -0.5x^2), \tag{4a}$$

where

$$x = (E - E_0)/\gamma, \tag{4b}$$

$\Phi(a,b,z)$ is the confluent hypergeometric function, and $A$ and $B$ are constants related to the optical matrix element of the transition and the relative contributions of band gap ($A$) and linewidth ($B$) dispersion to the signal, respectively.

Quantitative analysis of the ER spectra is dependent on the proper choice of line shape and also a close correspondence between the experimental conditions and the theoretical assumptions of dielectric function modulation in the derivation of the line shape. Our use of *p-i-n* diode samples ensures a constant homogeneous electric field across the QWs, in contrast to other similar experimental techniques such as photoreflectance, where the highly inhomogeneous fields induced across the QWs may compromise a quantitative analysis. The well-controlled field modulation in our experimental configuration directly correlates the ER signal with the assumed band gap and linewidth dispersion characteristics included in Eq. (4)

Figure 3 shows ER spectra taken at room temperature from the series of annealed GaInNAsSb QWs of Fig. 2. The spectrum from the as-grown sample is reproduced in Fig. 4(a), showing a series of oscillators fit with Eq. (4). The main feature around 0.785 eV arises from transitions across the fundamental gap between the first heavy hole (HH1) and electron levels, while the smaller features around 0.9 eV arise from both light hole (LH1) and HH2 transitions. (The nature of the transitions was determined by the direction of

their shifts with applied dc bias as well as comparison with calculated energies.) The large separation and spectral independence of the HH1 and LH1 features is clearly seen.

While at first glance the spectrum appears to consist of single lines for each HH and LH transition, a very poor fit results from using only one oscillator, even if a line shape different from Eq. (4) is used. However, careful fitting with multiple oscillators enables excellent fitting over the entire measurement range, as demonstrated in Fig. 4(a). Care in the fitting procedure is essential to ensure the parameters of the fitted lines do not diverge to unreasonable values and that extraneous lines are not included. The minimum number of oscillators to achieve an excellent fit was always used and attention was paid to parameters such as linewidth during the fitting. Indeed, the procedure for fitting the multiple oscillators proved nontrivial. Nonetheless, transition energies could be determined and, without *a priori* assumption, were found to match closely with the peak positions measured by PL [see Fig. 4(b)]. Further refinement of the fits, taking into account the PL results, allowed accurate determination of the fitting parameters for all of the nearest-neighbor states in each sample. Consistent with the PL and PC measurements, the strongest transitions had FWHM of 20–25 meV, while very weak transitions showed broadening up to 40–50 meV.

In Eq. (4a), the relative magnitudes of $A$ and $B$ can be understood to represent a phase factor, so the total amplitude of the transition can be taken as the quadrature sum:

$$C = \sqrt{A^2 + B^2}. \tag{5}$$

Since the states have approximately the same intrinsic matrix element, the relative amplitudes of the nearest-neighbor transitions can be used to directly determine the distribution of nearest-neighbor states in the material. These distributions are plotted in Fig. 4(c) for the as-grown and variously annealed samples. Also plotted in Fig. 4(c) is the calculated distribution for a random arrangement of atoms in material having the same In and N composition as these samples. A correspondence is clearly seen between the random distribution and the distribution measured for the as-grown sample, confirming the kinetic nature of the low-temperature growth. As the material is annealed, the less-thermodynamically-favored $N^{(0)}$ and $N^{(1)}$ states are quickly depleted and high In coordinations become dominant. Here we have introduced the notation $N^{(n)}$, in analogy with the $GaInNAs^{(n)}$ notation, to denote a N environment with $n$ In nearest neighbors irrespective of the host material (i.e., GaInNAs or GaInNAsSb).

### D. Photocurrent (PC)

Figure 5 summarizes the photocurrent results from the same GaInNAsSb samples used in the PL and ER experiments. The raw responsivity data was converted to absorption coefficient in the figure. The wavelength region shown only includes the HH1 transitions. The excitonic peaks in the absorption spectra were well fit by a Gaussian line shape with FWHM ~25 meV, consistent with the results presented above.

The spectra clearly show discrete peaks corresponding to the transitions found in PL and ER, which are indicated by the vertical lines in the figure, and the higher energy states are seen to grow as the material is annealed. Similar to the PL results, we see discrete jumps between the states, but unlike PL which is dominated by the lowest energy transition, the PC results show us the relative strengths of the transitions. Particularly interesting is that for the as-grown sample the PL shows a dominant peak at the $N^{(0)}$ position, while in PC only a small shoulder appears for $N^{(0)}$ and the dominant peak is at $N^{(1)}$ [Fig. 5(a)]. As the $N^{(1)}$ state anneals out, the $N^{(2)}$ state becomes dominant. As the annealing proceeds, the absorption also becomes stronger, as both the material quality improves (evidenced by the sharpening of the exciton peaks) and also more optically efficient higher In coordinated states appear.

## IV. DISCUSSION

The five peaks observed in the PL spectra correspond to the five possible N-In nearest-neighbor configurations in GaInNAs(Sb). The ER and PC results further corroborate this conclusion and also show precisely how the nearest-neighbor bonding changes while annealing, in tandem with the PL blueshift. While the presence of Sb, a Group V element, does not play a direct role in the N nearest-neighbor bonding in GaInNAsSb, the energy spacing between the nearest-neighbor states is found to be about 50% smaller than for GaInNAs. Our calculations for GaInNAs with comparable N content predicts an average energy spacing of ~34 meV per In atom,[22] and measurements have found a spacing of ~40 meV or more.[11] However, our measurements of GaInNAsSb in this work indicate a spacing of ~18 meV.

Although Sb contributes to band gap lowering in GaInNAsSb due to the small band gaps of the binary antimonides, nitrogen bonding still dominates the band edge states of GaInNAsSb, as in GaInNAs. The two main effects of Sb incorporation, in addition to the incidental band gap lowering, are improvement in material/interface quality through the reactive surfactant effect of Sb (Ref. 28) and increase of the valence band offset between QW and barrier. Being a Group V element, Sb does not directly influence the N bonding in the material, although an enhancement of N incorporation from the presence of Sb has been observed.[29–31] The precise effect of Sb as both a surfactant and incorporant in GaInNAsSb is complex and not fully understood. Certainly, there are contributions to the attachment and diffusion rate of species (e.g., N and In) on the surface during growth. Nevertheless, the random distribution of as-deposited bonds is not affected by the presence of Sb at these low growth temperatures, as evidenced by the ER results and Fig. 4(c).

The saturation of the PL blueshift with increased annealing (temperature, time, or both) is very important for the practical use of GaInNAs(Sb) in optoelectronic devices such as vertical cavity surface emitting lasers (VCSELs). The ability to accurately and reliably predict the peak gain wavelength (related to the peak PL wavelength) is necessary to allow matching to the VCSEL cavity and specification of the

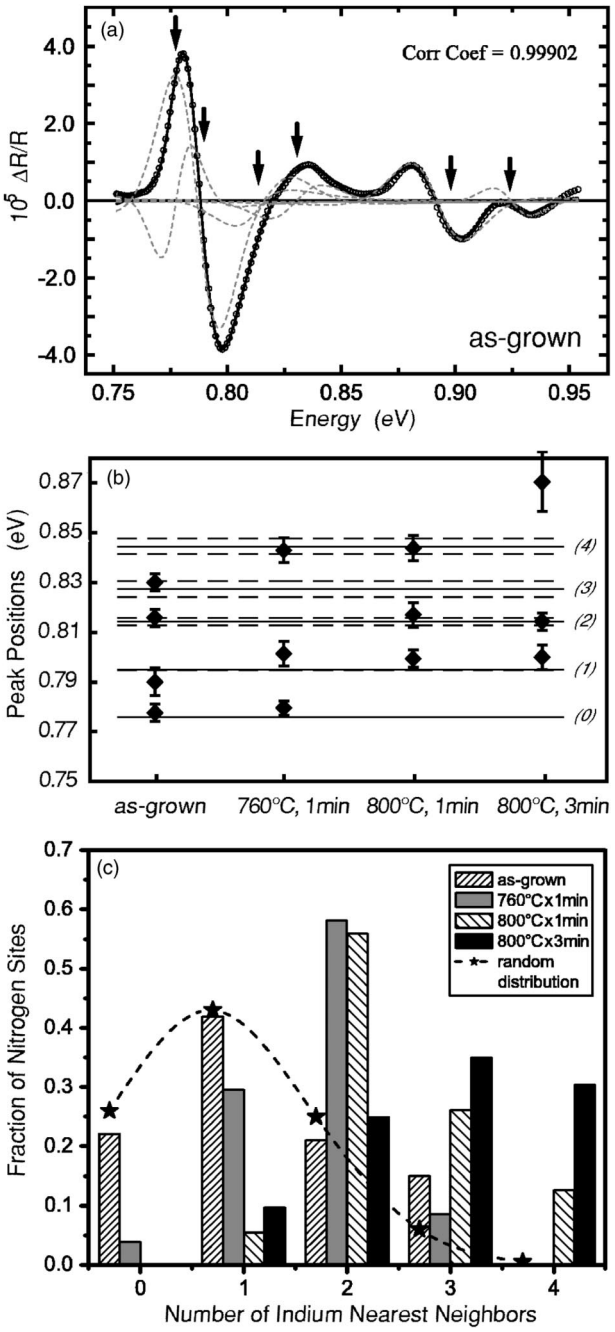


FIG. 4. (a) Room-temperature electroreflectance spectrum from as-grown GaInNAsSb QW (circles) and theoretical fit (solid curve). Dashed curves show the individual oscillator fits, while arrows indicate the transition energies. (b) Dominant peak positions for HH1 to conduction band transitions obtained by ER (symbols) plotted against the peak fit positions from PL (horizontal lines). The numbers in parentheses indicate the number of In nearest neighbors to N, as in Fig. 2. (c) Distribution of N-In nearest-neighbor bonding obtained from the amplitude of the ER fits (bars). Stars indicate the calculated distribution for random bonding, which agrees well with the measurement for as-grown material.

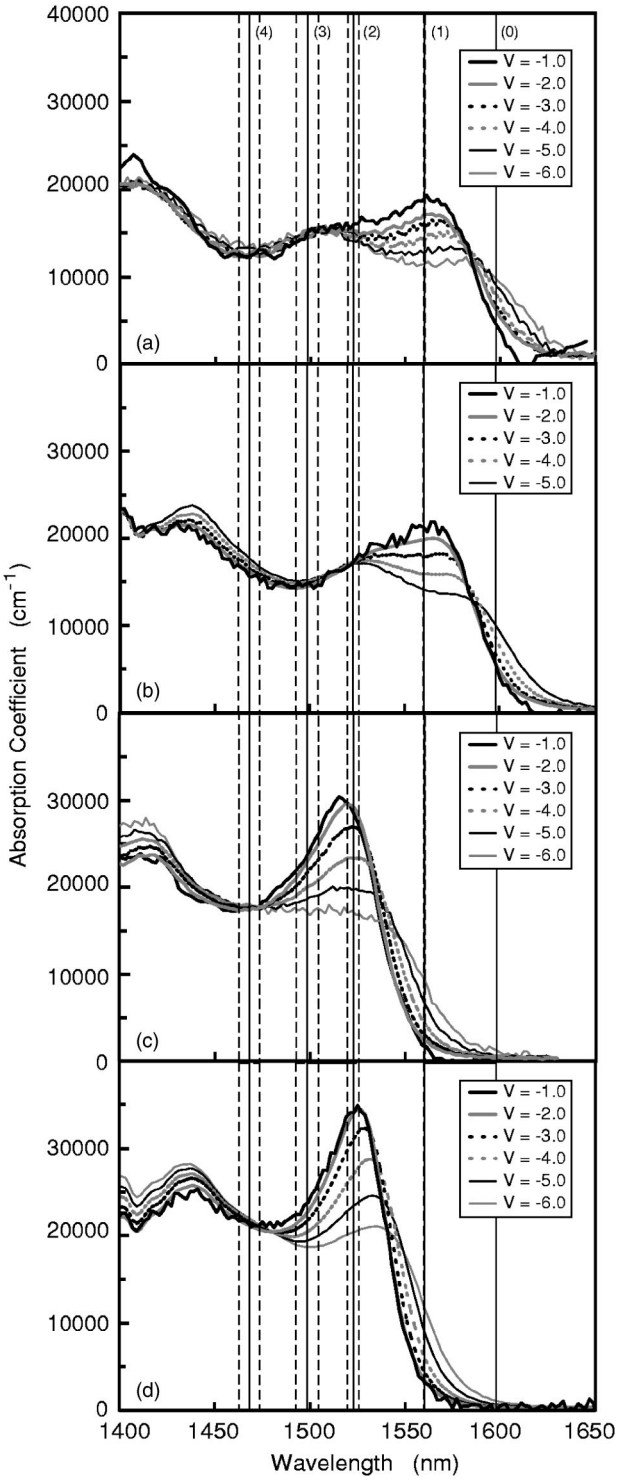


FIG. 5. Absorption spectra of GaInNAsSb QWs around the band edge region taken with photocurrent, for (a) as-grown, (b) annealed 760 ° C for 1 min, (c) annealed 800 ° C for 1 min, and (d) annealed 800 ° C for 3 min. The vertical lines indicate the peak fit positions from PL, from Fig. 2.

operating wavelength. In the past, this has been difficult to achieve since annealing and other thermal processing would result in potentially unknown amounts of wavelength shift. However, if the material is "fully" annealed, the wavelength will be stable and, furthermore, the amount of the shift from as-grown material can be predicted. Steps may need to be taken to prevent degradation of PL intensity at the highest annealing temperatures/times ("rollover"), which sometimes

is observed. The precise mechanism of this degradation is not well understood, but probably has to do with activation of some point defect or in-diffusion of vacancies from the wafer surface. Thick cap layers (which are inherently a part of laser structures) and high quality interfaces seem to mitigate this effect.

These results interestingly show that "partially" annealed material is indeed possible. From a technological point of view, the fully annealed state is the most ideal for device design, as described above; however, comparing the PL and ER results, we can see that even when the PL wavelength apparently has saturated, the nearest-neighbor distributions may still change. Also, it is not clear what the final equilibrium distribution should be; the distribution from ER for the furthest annealed sample shows a sort of equalization of the $N^{(2)}, N^{(3)}$, and $N^{(4)}$ states. We also note that early in the annealing process, the $N^{(0)}$ and $N^{(1)}$ states are quickly diminished to very low levels. This is consistent with our calculations shown in Fig. 1(c) of Ref. 9, where the greatest drop in the total energy of the system occurs between the $N^{(1)}$ and $N^{(2)}$ states. Additionally, while ER is a technique well suited to measuring excited states and thus was able to produce the distributions shown in Fig. 4(c), PL is most sensitive to the lowest energy transition in the system, since the intraband carrier relaxation rates are much higher than the spontaneous recombination rates and the thermal population of excited states is exponentially lower than the ground-state population. Thus, the most dramatic shifts in the PL spectra are observed when a lower energy state essentially disappears. By examining Figs. 2 and 4(c), we can see that after annealing at 760 °C for 1 min, the as-grown sample lost essentially all of the $N^{(0)}$ states and produced a correspondingly large shift in the PL. Similarly, the sample annealed at 800 °C for 1 min showed an additional discrete shift in PL as the $N^{(1)}$ state was depleted. However, all of the samples show significant populations of the $N^{(2)}$ state, and no significant further shift is clearly observed in PL after annealing at 800 °C for 1 min. Furthermore, the peaks in PL are spaced very close together ($\sim$18 meV) compared to their full widths ($\sim$25 meV), so small changes in the nearest-neighbor distributions would not be grossly apparent, as in the case between the samples annealed at 800 °C for 1 and 3 min. A further point is that, as the material is annealed, the PL intensity increases due to the removal of nonradiative recombination centers, but some of the intensity increase is attributable to the increased N-In bonding, according to our band-structure calculations,[9,22] the x-ray absorption/emission experiments of Strocov *et al.*,[15] and our PC measurements.

In contrast to both PL and ER, PC spectra show features mainly sensitive to the relative oscillator strengths of the measured transitions (in addition to the distribution of the states). Thus, the PC data enables us to determine the strongest transitions in each sample and relate them to the nearest-neighbor distributions. The data in Fig. 5, when compared with Fig. 4(c), show that the $N^{(0)}$ state has a small oscillator strength, since even with significant population of the $N^{(0)}$ state in the as-grown material [Fig. 4(c)], the absorption spectrum is strongly peaked at the $N^{(1)}$ position and shows only a small kink for the $N^{(0)}$ state [Fig. 5(a)]. On the other hand, the states with at least 1 N-In nearest neighbor show considerably higher transition strengths (especially $N^{(2+)}$). Furthermore, as annealing removes the less-optically-efficient low-In coordinated N states, the absorption coefficient is increased at the band edge, as seen in the PC data with increasing anneal. This is in addition to improvements in material quality, demonstrated by the narrowing of the exciton linewidth.

## V. CONCLUSIONS

Near-edge x-ray absorption fine structure measurements on compressively strained thin-films of GaInNAs grown on GaAs show that the biaxial compressive strain does not affect the N-In nearest-neighbor distribution in this material, compared with unstrained thick films studied previously. As in the thick films, as-grown material was found to have a nearly random bond distribution peaked around one N-In nearest neighbor, while annealed material moved toward a more thermodynamically favored distribution peaked at two to three N-In nearest neighbors. Thus, the strain present in technologically relevant material for use in the 1.3–1.6 μm wavelength region does not significantly affect the bonding properties or annealing kinetics of the material.

Furthermore, we found a series of states at the band edge of GaInNAsSb that are consistent with N-In nearest-neighbor states, as found in GaInNAs. The presence of Sb, a Group V element, does not alter the N bonding environment directly, although it plays some role in the growth kinetics of the material. The splitting between the nearest-neighbor states in GaInNAsSb was found to be significantly smaller ($\sim$18 meV) than in GaInNAs ($\sim$35 meV). Nevertheless, as-grown GaInNAsSb still was found to contain a nearly random distribution of nearest-neighbor bonds.

The nearest-neighbor splittings were observed in photoluminescence, optical absorption (photocurrent), and electroreflectance experiments, up to room temperature. The line shape observed in all cases was found to be Gaussian, with a FWHM $\sim$25 meV at room temperature, indicating a strong exciton-phonon coupling. Careful peak fitting of the ER data enabled distributions of bonding states to be determined directly from the relative amplitudes of the oscillator fits. The distributions illustrate the shift from near-random N-In bonding after growth to high-In coordinated N bonds as the material is annealed. As the nearest-neighbors reconfigure toward increased numbers of N-In bonds, the band gap blueshifts accordingly, but eventually saturates when the fully annealed, thermodynamic equilibrium distribution is achieved. However, the band gap measured by PL, which is most sensitive to the lowest energy transition, only shows a strong shift when a nearest-neighbor state is almost fully depleted, which occurs rather quickly for the $N^{(0)}$ and $N^{(1)}$ states. The increased N-In bonding also contributes somewhat to the increased luminescence and absorption observed after annealing.

Photocurrent measurements of the absorption spectra of the GaInNAsSb QWs highlight the relative oscillator strengths of the observed transitions. The $N^{(0)}$ state was found to have much weaker optical activity than the others. As annealing drives the introduction of additional N-In

bonds, the optical efficiency of the material improves, in addition to the improvement from removal of nonradiative defects in this low-temperature material. Regarding grown-in nonradiative defects, GaInNAsSb is of higher quality than GaInNAs, since the surfactant property of Sb improves the as-grown material quality and interface smoothness. Consequently, the PL efficiency and absorption coefficient of as-grown GaInNAsSb is appreciably higher than for as-grown GaInNAs.[7] Additionally, the higher electron effective mass in the antimonide contributes to a higher value of absorption coefficient for GaInNAsSb relative to GaInNAs.

### Acknowledgments

Support was provided by DARPA/ONR through Grant No. MDA972-00-1-0024 and by the Stanford Network Research Center. V.L. also thanks the Fannie and John Hertz Foundation for financial support.

*Electronic address: vlordi@snow.stanford.edu

[1] M. Kondow, K. Uomi, A. Niwa, T. Kitatani, S. Watahiki, and Y. Yazawa, Jpn. J. Appl. Phys., Part 1 **35**, 1273 (1996).
[2] J. S. Harris, Jr., Semicond. Sci. Technol. **17**, 880 (2002).
[3] J. S. Harris, Jr., IEEE J. Sel. Top. Quantum Electron. **6**, 1145 (2000).
[4] H. Riechert, A. Ramakrishnan, and G. Steinle, Semicond. Sci. Technol. **17**, 892 (2002).
[5] S. R. Bank, M. A. Wistey, L. L. Goddard, H. B. Yuen, V. Lordi, and J. S. Harris, IEEE J. Quantum Electron. **40**, 656 (2004).
[6] M. A. Wistey, S. R. Bank, H. B. Yuen, L. L. Goddard, and J. S. Harris, Electron. Lett. **39**, 1822 (2003).
[7] V. Lordi, H. Yuen, S. Bank, and J. S. Harris, Appl. Phys. Lett. **85**, 902 (2004).
[8] W. Ha, V. Gambin, S. Bank, M. Wistey, H. Yuen, V. Lordi, S. Kim, and J. S. Harris, Jr., IEEE J. Quantum Electron. **38**, 1260 (2002).
[9] V. Lordi, V. Gambin, S. Friedrich, T. Funk, T. Takizawa, K. Uno, and J. S. Harris, Phys. Rev. Lett. **90**, 145505 (2003).
[10] K. Kim and A. Zunger, Phys. Rev. Lett. **86**, 2609 (2001).
[11] P. J. Klar, H. Grüning, J. Koch, S. Schäfer, K. Volz, W. Stolz, W. Heimbrodt, A. M. Kamal Saadi, A. Lindsay, and E. P. O'Reilly, Phys. Rev. B **64**, 121203(R) (2001).
[12] S. Kurtz, J. Webb, L. Gedvilas, D. Friedman, J. Geisz, J. Olson, R. King, D. Joslin, and N. Karam, Appl. Phys. Lett. **78**, 748 (2001).
[13] T. Kitatani, M. Kondow, and M. Kudo, Jpn. J. Appl. Phys., Part 2 **40**, L750 (2001).
[14] H. C. Alt, A. Y. Egorov, H. Riechert, B. Wiedemann, J. D. Meyer, R. W. Michelmann, and K. Bethge, Physica B **302-303** , 282 (2001).
[15] V. N. Strocov, P. O. Nilsson, T. Schmitt, A. Augustsson, L. Gridneva, D. Debowska-Nilsson, R. Claessen, A. Y. Egorov, V. M. Ustinov, and Z. I. Alferov, Phys. Rev. B **69**, 035206 (2004).
[16] A. T. Young, V. Martynov, and H. A. Padmore, J. Electron Spectrosc. Relat. Phenom. **101-113**, 885 (1999).
[17] S. Friedrich, T. Funk, O. Drury, S. E. Labov, and S. P. Cramer, Rev. Sci. Instrum. **73**, 1629 (2002).
[18] V. Lordi, S. Friedrich, and J. S. Harris (unpublished).
[19] S. G. Spruytte, C. W. Coldren, J. S. Harris, W. Wampler, P. Krispin, K. Ploog, and M. C. Larson, J. Appl. Phys. **89**, 4401 (2001).
[20] S. G. Spruytte, Ph.D. thesis, Stanford University, 2001.
[21] W. Ha, V. Gambin, S. Bank, M. Wistey, H. Yuen, V. Lordi, S. Kim, and J. S. Harris, Jr., IEEE J. Quantum Electron. **38**, 1260 (2002).
[22] V. Lordi and J. S. Harris (unpublished).
[23] H. B. Bebb and E. W. Williams, in *Transport and Optical Phenomena*, edited by R. K. Willardson and A. C. Beer, *Semiconductors and Semimetals* Vol. 8 (Academic Press, New York, 1972), chap. 4, p. 200ff.
[24] Y. Toyozawa, Prog. Theor. Phys. **20**, 53 (1958).
[25] M. Cardona, *Modulation Spectroscopy* (Academic Press, New York, 1969).
[26] B. V. Shanabrook, O. J. Glembocki, and W. T. Beard, Phys. Rev. B **35**, 2540 (1987).
[27] H. Shen, S. H. Pan, F. H. Pollak, M. Dutta, and T. R. AuCoin, Phys. Rev. B **36**, 9384 (1987).
[28] J. Massies and N. Grandjean, Phys. Rev. B **48**, 8502 (1993).
[29] L. H. Li, V. Sallet, G. Patriarche, L. Largean, S. Bouchoule, K. Merghem, L. Travers, and J. C. Harmand, Electron. Lett. **39**, 519 (2003).
[30] K. Volz, V. Gambin, W. Ha, M. A. Wistey, H. B. Yuen, S. R. Bank, and J. S. Harris, J. Cryst. J. Cryst. Growth **251**, 360 (2003).
[31] H. B. Yuen, S. R. Bank, M. A. Wistey, A. Moto, and J. S. Harris, J. Appl. Phys. **96**, 6375 (2004).